Ca-Sr fractionation between zoisite, lawsonite and aqueous fluids - An experimental study at 2.0 and 4.0 GPa/400 to 800 °C

- REVISION 2 -

A. LIEBSCHER,[1,2,*] G. DÖRSAM,[2] G. FRANZ,[2] B. WUNDER,[1] AND M. GOTTSCHALK[1]

[1]German Research Centre for Geosciences GFZ Potsdam, Telegrafenberg, D-14473 Potsdam, Germany

[*]Email: alieb@gfz-potsdam.de

[2]Fachgebiet Mineralogie-Petrologie, Technische Universität Berlin, Ackerstr. 76, D-13355 Berlin, Germany

ABSTRACT

The Ca-Sr fractionation between zoisite respectively lawsonite and an aqueous fluid has been determined by synthesis experiments in the presence of a 1 M (Ca,Sr)Cl_2 aqueous fluid at 2.0 GPa/550, 600, and 700 °C and 4.0 GPa/800 °C for zoisite, and 2.0 GPa/400 °C and 4.0 GPa/600 °C for lawsonite. Solid run products were characterized by EMP, SEM and XRD with Rietveld refinement and fluids were analysed by ICP-OES. Zoisite exhibits notable intracrystalline Ca-Sr fractionation between the A1 and A2 sites and calculated intracrystalline exchange coefficients $K_{D(Sr-Ca)}^{A1-A2}$ = 1.5 to 26 show strong preference of Sr over Ca for the slightly larger A2 site. Calculated individual site dependent zoisite-aqueous fluid exchange coefficients for the studied 1 M (Ca,Sr)Cl_2 aqueous fluids are $K_{D(Sr-Ca)}^{zoisite\ A1-aqueous\ fluid}$ = 3.38 to 41.08 for the A1 site and $K_{D(Sr-Ca)}^{zoisite\ A2-aqueous\ fluid}$ = 0.45 to 6.51 for the A2 site. Assuming $\gamma_{Ca}^{\text{aqueous fluid}} = \gamma_{Sr}^{\text{aqueous fluid}}$ and a symmetric mixing model, the thermodynamic evaluation of the site dependent exchange reactions $Ca^{2+\text{ (aqueous fluid)}}$ + $Sr^{A1}(M^{2+})^{A2}Al_3[Si_3O_{11}(O/OH)] = Sr^{2+\text{ (aqueous fluid)}} + Ca^{A1}(M^{2+})^{A2}Al_3[Si_3O_{11}(O/OH)]$ and $Ca^{2+\text{ (aqueous fluid)}} + (M^{2+})^{A1}Sr^{A2}Al_3[Si_3O_{11}(O/OH)] = Sr^{2+\text{ (aqueous fluid)}} + (M^{2+})^{A1}Ca^{A2}Al_3[Si_3O_{11}(O/OH)]$ yields $\Delta\mu^0$ = -29 kJ/mol and $W_{Sr-Ca}^{zoisite\ A1}$ = 5.5 kJ/mol for the A1 site and $\Delta\mu^0$ = -1.1 kJ/mol and $W_{Sr-Ca}^{zoisite\ A2}$ = 0 kJ/mol for the A2 site at P and T of the experiments. The data indicates ideal Ca-Sr substitution on the A2 site. Lawsonite formed in both the orthorhombic *Cmcm* and the monoclinic *P2₁/m* form. Calculated lawsonite-aqueous fluid exchange coefficients indicate overall preference of Ca over Sr in the solid and are $K_{D(Sr-Ca)}^{lawsonite\ Cmcm-aqueous\ fluid}$ = 1.12 to 11.32 for orthorhombic and $K_{D(Sr-Ca)}^{lawsonite\frac{P21}{m}-aqueous\ fluid}$ = 1.67 to 4.34 for monoclinic lawsonite. Thermodynamic evaluation of the exchange reaction $Ca^{2+\text{ (aqueous fluid)}}$ + $SrAl_2Si_2O_7(OH)_2{\bullet}H_2O = Sr^{2+\text{ (aqueous fluid)}} + CaAl_2Si_2O_7(OH)_2{\bullet}H_2O$ assuming $\gamma_{Ca}^{\text{aqueous fluid}} = \gamma_{Sr}^{\text{aqueous fluid}}$ and a symmetric mixing model yields similar values of $\Delta\mu^0$ = -9 kJ/mol and $W_{Sr-Ca}^{lawsonite\ Cmcm}$ = 10 kJ/mol for orthorhombic

and $\Delta\mu^0$ = -10 kJ/mol and $W_{Sr-Ca}^{lawsonite\ P21/m}$ = 11 kJ/mol for monoclinic lawsonite. Calculated Nernst distribution coefficients for the studied 1 M $(Ca,Sr)Cl_2$ aqueous fluids are $D_{Sr}^{\text{zoisite-aqueous fluid}} = 2.8 \pm 0.7$ for zoisite at 2 GPa/600 °C and $D_{Sr}^{\text{lawsonite } Cmcm\text{-aqueous fluid}} = 0.6 \pm 0.2$ for orthorhombic lawsonite at 4 GPa/600 °C and show Sr to be compatible in zoisite but incompatible in lawsonite. This opposite mineral-aqueous fluid fractionation behavior of Sr with respect to zoisite and lawsonite on the one hand and the ideal Ca-Sr substitution on the zoisite A2 site in combination with the strong intracrystalline Ca-Sr fractionation in zoisite on the other hand make Sr a potential tracer for fluid-rock interactions in zoisite- and lawsonite-bearing rocks. For low Sr-concentrations, x_{Sr}^{zoisite} directly reflects $x_{Sr}^{\text{aqueous fluid}}$ and allows calculate Sr-concentrations in the metamorphic aqueous fluid. During high-pressure aqueous fluid-rock interactions in subduction zone settings the opposite mineral-aqueous fluid fractionation behavior of Sr results in different aqueous fluid characteristics for lawsonite- versus zoisite-bearing rocks. Ultimately, subduction zone magmas may trace these different aqueous fluid characteristics and allow distinguishing between cold, lawsonite-bearing versus hot, zoisite-bearing thermal regimes of the underlying subduction zone.

INTRODUCTION

The concentration of strontium and especially its enrichment in metamorphic rocks and minerals are potential tracers of metamorphic fluid-rock interactions and metasomatic processes (Grapes and Watanabe 1984). An extreme example of such fluid-induced Sr metasomatism is, e.g., reported by Brastadt (1985) from a metaeclogite from Bjørkedalen, Norway. Because the ionic radii of Ca^{2+} (= 1.06 Å) and Sr^{2+} (= 1.21 Å; both for sevenfold coordination; Shannon 1976) are quite similar Sr readily substitutes for Ca. Besides carbonates, the Ca-silicates plagioclase and members of the epidote and lawsonite groups are therefore the most important carriers of Sr in typical metamorphic rocks. In high- and ultrahigh-pressure metabasites and metagreywackes, minerals of the epidote and lawsonite groups, which replace the anorthite component of plagioclase in the protoliths, may control more than 75% of the whole-rock Sr budget (Tribuzio et al. 1996; Nagasaki and Enami 1998; Zack et al. 2002; Spandler et al. 2003). The geochemical cycles of Sr in subduction zone settings and in high-pressure regional metamorphism are therefore largely controlled by the fractionation behavior of Sr between epidote minerals, lawsonite und metamorphic fluids although also carbonates may play an important role. Knowledge of this fractionation behavior provides the potential to use Sr concentrations as tracer of prograde dehydration reactions or breakdown reactions of the respective carrier minerals of the epidote and lawsonite groups. Potential differences in Ca-Sr fractionation between zoisite-aqueous fluid and lawsonite-aqueous fluid may also be traced in the compositions of arc magmas generated at subduction zones and may allow deciphering the thermal regime of the underlying subduction zone, e.g. cold, lawsonite-bearing settings versus warm, zoisite-bearing settings. Recently, the trace element fractionation of Sr between zoisite and aqueous fluid has been studied by Feineman et al. (2007) at 750 to 900 °C/2.0 GPa and between zoisite and lawsonite and aqueous fluid by Martin et al. (2011) at 650 to 850 °C/3.0 to 3.5 GPa. Both studies found Sr to be compatible in zoisite; however, the calculated Nernst distribution coefficients

$D_{Sr}^{\text{zoisite-aqueous fluid}} = c_{Sr}^{\text{zoisite}}/c_{Sr}^{\text{aqueous fluid}}$ are notably higher in Feineman et al. (2007) with $D_{Sr}^{\text{zoisite-aqueous fluid}} = 42 \pm 18$ to 170 ± 80 than in Martin et al. (2011) with $D_{Sr}^{\text{zoisite-aqueous fluid}} = 2.2 \pm 0.3$ to 3.6 ± 1.2. Contrary to zoisite, the data for lawsonite by Martin et al. (2011) indicate that Sr is incompatible in lawsonite with $D_{Sr}^{\text{lawsonite-aqueous fluid}} = 0.14 \pm 0.02$ to 0.20 ± 0.02. However, epidote minerals and lawsonite not only incorporate Sr as a trace element but also as minor and even major element leading to extensive Ca-Sr solid solutions series (Dörsam et al. 2007; Liebscher et al. 2010); clinozoisite-(Sr) $Sr_2Al_3[SiO_4Si_2O_7(O/OH)]$ has been described by Miyajima et al. (2002) and the Sr-analogue of lawsonite itoigawaite $SrAl_2Si_2O_7(OH)_2 \bullet H_2O$ by Miyajima et al. (1999). The Nernst distribution coefficient is only applicable where Henry´s law is fulfilled, typically at low concentrations. Although the Henry´s law region may extend to higher concentrations for similar substituents as in the case of Ca and Sr, the fractionation behavior of Sr between aqueous fluids and members of the epidote and lawsonite groups is not adequately described by classical Nernst distribution coefficient. Instead, to describe the fractionation behavior of Sr as minor or even major element and to cover the complete solid solution series fractionation behavior has to be expressed via the equilibrium constant *K*. This approach then also allows deriving Ca-Sr mixing properties for the solid solution series (e.g., Najorka et al. 1999).

The data presented here form part of a larger on-going study on the Ca-Sr fractionation between solids and aqueous fluids at metamorphic conditions (e.g., Najorka et al. 1999; Dörsam et al. 2007; Liebscher et al. 2009, 2010). The crystal-structural and crystal-chemical aspects of the Ca-Sr substitution along the solid solution series $Ca_2Al_3[SiO_4Si_2O_7(O/OH)]$ - $Sr_2Al_3[SiO_4Si_2O_7(O/OH)]$ and $CaAl_2Si_2O_7(OH)_2 \bullet H_2O$ - $SrAl_2Si_2O_7(OH)_2 \bullet H_2O$ have been experimentally studied and described in detail by Dörsam et al. (2007) and Liebscher et al. (2010), respectively. Here we present fluid data and the calculated solid-aqueous fluid fractionation of Ca and Sr between zoisite, lawsonite and aqueous fluid for the Dörsam et al. (2007) and Liebscher et al. (2010) data complemented by additional experiments. In addition

to the solid-aqueous fluid fractionation of Ca and Sr, the focus of this contribution lies on the Ca-Sr mixing properties for both solid solution series.

EXPERIMENTAL AND ANALYTICAL METHODS

Detailed descriptions of experimental and analytical methods are given in Dörsam et al. (2007) and Liebscher et al. (2010) and are summarized here only briefly. Table 1 compiles all runs and the respective run conditions. Compositions of zoisite and lawsonite as determined by EMP are listed in Dörsam et al. (2007) and Liebscher et al. (2010), respectively.

Experimental techniques

Solid starting materials were prepared from oxide-hydroxide mixtures of α-quartz (ignited, Fe-free p.a. Merck), γ-Al_2O_3 (Aldrich), $Ca(OH)_2$, and either $SrSiO_3$ or $Sr(OH)_2•8H_2O$; $SrSiO_3$ was derived by heating $SrCO_3$ and quartz for ≈ 24 h at 1100°C. Depending on P-T run conditions and the targeted stable product phases (zoisite and/or lawsonite), solid starting material was weighed in stoichiometric amounts of the desired composition of either $(Ca,Sr)_2Al_3Si_3O_{11}(O/OH)$ or $(Ca,Sr)Al_2Si_2O_7(OH)_2•H_2O$. To account for preferred dissolution of SiO_2 into the aqueous fluid and to ensure quartz/coesite saturation of the run products, ~ 3.0 to 10 mol% excess SiO_2 were added to each run. The Ca-Sr composition is expressed as mol-fraction of the Sr component with $x_{Sr} = n_{Sr}/(n_{Sr}+n_{Ca})$. The solid starting material had bulk compositions from x_{Sr}^{bulk} = 0.02 to 0.95. To overcome kinetic problems and to allow for simple homovalent Ca-Sr fractionation between solids and aqueous fluid (Zimmermann et al. 1996), a 1 M $(Ca,Sr)Cl_2$ aqueous solution was added to each run; initial $x_{Sr}^{aqueous\ fluid}$ was identical to x_{Sr}^{bulk}. The initial solid-to-fluid ratio $(n_{Sr}+n_{Ca})^{aqueous\ fluid}/[(n_{Sr}+n_{Ca})^{aqueous\ fluid} + (n_{Sr}+n_{Ca})^{solid}]$ was variable between 0.019 and 0.523.

Starting mixtures of solids and aqueous fluid were sealed in Au or Pt capsules of 10 to 13 mm length, 2 mm diameter and 0.115 mm wall thickness and placed in NaCl assemblies with steel

132 furnaces following Massonne and Schreyer (1986). Using steel furnace assemblies provides
133 larger inner cell space compared to graphite furnaces and allows loading up to 4 capsules (2
134 mm in diameter) in a common assembly for the used ½ inch design. The steel furnace cell
135 design has been pressure calibrated via the two equilibria albite = quartz + jadeite and quartz
136 = coesite. Experiments were performed at 2.0 GPa/550, 600, and 700 °C and 4.0 GPa/800 °C
137 for zoisite experiments and 2.0 GPa/400 °C and 4.0 GPa/600 °C for lawsonite experiments
138 using a standard piston-cylinder apparatus. Run durations ranged between 4 and 7 days. The
139 temperature was recorded online with a Ni-CrNi thermocouple placed closely adjoining the
140 center of the capsules with an accuracy of ±10 °C. Pressure was controlled within ±50 MPa
141 by a JUMO controller. The assemblies were first pressurized to either 1.8 or 3.0 GPa, then
142 heated to the desired run temperatures and finally pressurized to 2.0 or 4.0 GPa. Switching off
143 the furnace current quenched the samples to below 200 °C within less than 10 s. After
144 quenching, the capsules were cleaned, weight checked and opened immersed in distilled H_2O
145 to recover the run fluid. Solid run products were filtered several times through a filter of 10-16
146 μm porosity until clocking of the filter pores, keeping all the fine-grained material in the filter.
147 The filter was dried at 100 °C for 15 min and the solid products were recovered from the filter.
148 The recovered product fluids were diluted to 50 ml with distilled H_2O.
149
150 **Analytical methods**
151 Solid run products were characterized by scanning electron microscopy (SEM), electron
152 microprobe (EMP), and X-ray diffraction (XRD) with Rietveld refinement. Scanning electron
153 microscopy images of the synthesis products were obtained with a Hitachi-S2700 instrument.
154 The composition of the solid phases was analyzed with a Cameca SX 50 microprobe on
155 polished and carbon coated samples using wavelength dispersive spectrometry, an
156 acceleration voltage of 10 kV, a beam current of 15.2 nA, and a beam diameter of 1 μm.
157 Counting time for all elements was 16 s on the peak position and 8 s on each side of the peak

158 for the background. The raw data were corrected with the PAP correction program (Pouchou
159 and Pichoir 1984). Using synthetic wollastonite (Si and Ca) and synthetic $SrAl_2Si_2O_8$ (Al and
160 Sr) as standards, AlK_α, SiK_β and SrL_β were analysed with a TAP crystal and CaK_α with a PET
161 crystal. Where possible, multiple analyses were done on single grains to check for
162 compositional homogeneity (see Dörsam et al. 2007; Liebscher et al. 2010).
163 For XRD with Rietveld refinement, sub-samples of the run products were ground in an agate
164 mortar for several minutes, diluted with Elmer's White glue and then evenly spread on a
165 circular foil. During drying, the powder was stirred to minimize preferred orientation. The foil
166 was covered with a second foil and placed into the transmission sample holder. Powder XRD
167 patterns were recorded in transmission between $2\Theta = 5°$ and 125° with a fully automated
168 STOE STADI-P diffractometer with $CuK_{\alpha1}$ radiation equipped with a primary
169 monochromator and a 7° wide position sensitive detector (PSD). Operation conditions of the
170 normal-focus Cu X-ray tube were 40 kV and 40 mA, using a take-off angle of 6°; detector
171 step size was 0.1° and resolution of 2Θ was 0.01°. Refinements were done with the GSAS
172 software package for Rietveld refinement (Larson and Von Dreele 1987). The peaks were
173 defined as pseudo-Voigt with variable Lorentzian character. The peak full-width at half
174 maximum height was varied as a function of 2Θ using the parameters *U*, *V*, and *W* of Caglioti
175 et al. (1958); for the Lorentzian character the parameters *X* and *Y* were used. The recorded
176 reflections were highly symmetric due to the geometry of the STADIP diffractometer and no
177 parameters describing the asymmetry of the peaks had to be used. The background was fitted
178 with a real space correlation function. Zoisite was refined in space group *Pnma* based on the
179 structural data for synthetic iron-free zoisite by Liebscher et al. (2002); lawsonite was refined
180 in space groups $P2_1/m$ for monoclinic (Ca,Sr)-lawsonite and *Cmcm* for orthorhombic (Ca,Sr)-
181 lawsonite, based on the structural data by Pawley and Allan (2001) for monoclinic lawsonite
182 and Libowitzky and Armbruster (1995) for orthorhombic lawsonite. The atomic displacement
183 parameters of lawsonite were fixed at the values from Libowitzky and Armbruster (1995).

Refinements were done in following sequence: scale factor, background, zero-point correction, phase fractions, lattice parameter, preferred orientation, profile parameter Cagliotti *W* and Lorentz *X*, atom parameters (excluding hydrogen), site occupancy with fractions of Ca and Sr for A1 and A2 positions in zoisite and A position in lawsonite, isotropic displacement parameters for zoisite, and remaining profile parameters Cagliotti *U* and *V* and Lorentz *Y*.

Calcium and Sr concentrations in the diluted (to 50 ml) product fluids were determined with a Vista-MPX CCD simultaneous ICP-OES in triplicate on lines 422.673 nm for Ca and 407.771 nm for Sr and averaged. Stabilization time applied was 20 s and 10 s were applied for sample uptake delay. Calibration was done with Specpure standard solutions from Alfar Aesar # 031852 for Ca and # 013874 for Sr. The relative error of the determined Ca and Sr concentrations is 3 % that of the calculated $x_{Sr}^{\text{aqueous fluid}}$ is 5 %. Because the capsules were opened "immersed" in distilled water and then filtered, no exact determination of mass of product fluid was possible. Concentrations of Ca and Sr in the un-diluted product fluid can therefore not be calculated. However, the masses [in mmol] of Sr and Ca in the un-diluted product fluid are given in Table 1 to allow for calculation of $x_{Sr}^{\text{aqueous fluid}}$.

RESULTS

Description of run products

Zoisite content in the 19 runs, which were used to constrain the Ca-Sr fractionation between zoisite and aqueous fluid (Table 1a) ranges from 12 to 100 wt% of the solid product phases. Additional phases include quartz in 2 GPa runs except for runs Au45 and Pt4 and coesite in 4 GPa runs, and variable amounts of clinozoisite, monoclinic and/or orthorhombic lawsonite, strontianite, kyanite, pyrophyllite, slawsonite and walstromite (Table 1a). Zoisite crystals are idiomorphic to hypidiomorphic with a short-prismatic habit of 1 to 10 μm width and 10 to 30 μm length and show typical orthorhombic morphology with {100}, {001}, {101} and {210} (Dörsam et al. 2007). The EMP analyses proved homogeneous zoisite composition within

each individual run as well as within individual zoisite crystals (Dörsam et al. 2007). However, following Dörsam et al. (2007) we will only refer to the Ca-Sr composition of zoisite determined by XRD in the following because EMP measurements do not distinguish between zoisite and clinozoisite in runs in which both polymorphs are present. Additionally, the XRD data allow determining the site-specific Ca-Sr composition on A1 and A2 sites of zoisite. Runs that lack clinozoisite proved the reliability of zoisite compositions determined by XRD by comparison with the EMP data (Dörsam et al. 2007). Zoisite composition ranges from $x_{Sr}^{zoisite} = 0.05 \pm 0.03$ to 0.87 ± 0.02 and covers nearly the complete solid solution series. Strontium concentration $x_{Sr}^{zoisite}$ shows a clear positive correlation with x_{Sr}^{bulk} but tends to be slightly smaller than the latter (Fig. 1a), whereas $x_{Sr}^{aqueous\ fluid}$ is generally higher than x_{Sr}^{bulk} (Fig. 1b).

The Ca-Sr fractionation between lawsonite and aqueous fluid has been determined based on 16 experiments (Table 1b). In the 2 GPa/400 °C runs lawsonite contents range from 43 to 51 wt% of the solid run products whereas in the 4 GPa/600 °C runs lawsonite yields are significantly higher and range from 82 to 99 wt% of the solid run products. All runs contain additional coesite (at 4 GPa) or quartz (at 2 GPa) except for runs Au63 and Au92. At 2 GPa/400 °C 13 to 15 wt% strontianite and 12 to 17 wt% diaspore formed. Other additional minor product phases in some runs include kyanite, wollastonite, and grossular. Lawsonite forms small, euhedral crystals typically below 10 μm in size. Lawsonite habit changes from more prismatic at low x_{Sr}^{bulk} to more isometric at higher x_{Sr}^{bulk} (Liebscher et al. 2010). Refinement of the XRD data shows that lawsonite formed in both the orthorhombic *Cmcm* and monoclinic $P2_1/m$ form depending on P-T conditions and x_{Sr}^{bulk}. Because EMP data do not distinguish between both polymorphs, we only refer to the Ca-Sr composition of lawsonite determined by XRD, following Liebscher et al. (2010). Strontium contents in orthorhombic lawsonite range from $x_{Sr}^{lawsonite\ Cmcm} = 0.02 \pm 0.01$ to 0.62 ± 0.05 whereas those in monoclinic lawsonite range from $x_{Sr}^{lawsonite\ P21/m} = 0.21 \pm 0.04$ to 0.97 ± 0.02. At 2 GPa/400

°C both forms coexist and the data suggest decreasing amounts of orthorhombic lawsonite but increasing amounts of monoclinic lawsonite with increasing x_{Sr}^{bulk}. At 4 GPa/600 °C lawsonite is exclusively orthorhombic at $x_{Sr}^{bulk} < 0.18$, exclusively monoclinic at $x_{Sr}^{bulk} > 0.45$ and both forms coexist in the compositional range $0.18 <$ at $x_{Sr}^{bulk} < 0.45$. As is the case at 2 GPa/400 °C, the data suggest that in this compositional range the amount of orthorhombic lawsonite decreases with increasing at x_{Sr}^{bulk} while that of monoclinic lawsonite increases. For runs that either contain orthorhombic or monoclinic lawsonite, XRD analyses agree well with the Ca-Sr composition of lawsonite as determined by EMP and proved lawsonite to be homogeneous within the individual runs as well as within individual crystals (Liebscher et al. 2010). The Ca-Sr composition of lawsonite corresponds to x_{Sr}^{bulk} although the data indicate overall slightly lower $x_{Sr}^{lawsonite}$ than x_{Sr}^{bulk} (Fig. 1c). Similarly as in the zoisite experiments, $x_{Sr}^{aqueous\ fluid}$ is generally higher than the corresponding x_{Sr}^{bulk} (Fig. 1d).

Intracrystalline Ca-Sr partitioning in zoisite

The new additional experiments fit well with the results by Dörsam et al. (2007) and prove the strong intracrystalline Ca-Sr fractionation in zoisite (Fig. 2). Strontium has a clear preference over Ca for the slightly larger A2 site (Liebscher et al. 2002; Dörsam et al. 2007). Up to about $x_{Sr}^{zoisite} = 0.4$ Sr substitutes for Ca almost exclusively on A2. The Sr contents on A1 are generally below $x_{Sr}^{zoisite\ A1} = 0.1$ within this compositional range while Sr contents on A2 linearly increase up to $x_{Sr}^{zoisite\ A2} = 0.66$ (Fig. 2a). Notable amounts of Sr on A1 are only observed for $x_{Sr}^{zoisite} > 0.4$ and $x_{Sr}^{zoisite\ A2} > 0.7$ (Fig. 2). The calculated intracrystalline exchange coefficient

$$K_{D(Sr-Ca)}^{A1-A2} = \frac{x_{Ca}^{A1} * x_{Sr}^{A2}}{x_{Sr}^{A1} * x_{Ca}^{A2}} \quad (1)$$

is generally > 1 reflecting the preferred substitution of Sr on A2. The calculated $K_{D(Sr-Ca)}^{A1-A2}$-values slightly scatter between 2 and 26, but most data suggest $K_{D(Sr-Ca)}^{A1-A2} = 10$ to 20 (Fig. 2b).

Ca-Sr fractionation between zoisite/lawsonite and aqueous fluid

The Ca-Sr fractionation between zoisite-aqueous fluid and lawsonite-aqueous fluid can be described by the general exchange reactions

$$2\ Ca^{2+\ (aqueous\ fluid)} + Sr_2Al_3[Si_3O_{11}(O/OH)] = 2\ Sr^{2+\ (aqueous\ fluid)} + Ca_2Al_3[Si_3O_{11}(O/OH)] \quad (2)$$

and

$$Ca^{2+\ (aqueous\ fluid)} + SrAl_2Si_2O_7(OH)_2{\bullet}H_2O = Sr^{2+\ (aqueous\ fluid)} + CaAl_2Si_2O_7(OH)_2{\bullet}H_2O. \quad (3)$$

To account for the two distinct A-positions in zoisite and the significant intracrystalline Ca-Sr fractionation between A1 and A2, reaction (2) has to be split into the site-specific exchange reactions

$$Ca^{2+\ (aqueous\ fluid)} + Sr^{A1}(M^{2+})^{A2}Al_3[Si_3O_{11}(O/OH)] = Sr^{2+\ (aqueous\ fluid)} + Ca^{A1}(M^{2+})^{A2}Al_3[Si_3O_{11}(O/OH)] \quad (2a)$$

and

$$Ca^{2+\ (aqueous\ fluid)} + (M^{2+})^{A1}Sr^{A2}Al_3[Si_3O_{11}(O/OH)] = Sr^{2+\ (aqueous\ fluid)} + (M^{2+})^{A1}Ca^{A2}Al_3[Si_3O_{11}(O/OH)]\ . \quad (2b)$$

The solid-aqueous fluid Ca-Sr fractionation for reactions (2) and (3) can then be described by $x_{Sr}^{aqueous\ fluid}$ versus $x_{Sr}^{mineral}$ diagrams (Figs 3a, 4), the site dependent zoisite-aqueous fluid Ca-Sr fractionation for reactions (2a) and (2b) by $x_{Sr}^{aqueous\ fluid}$ versus $x_{Sr}^{zoisite\ A1/A2}$ diagrams (Fig. 3b). Zoisite and lawsonite both exhibit overall preferred fractionation of Ca over Sr compared to the aqueous fluid (Figs 3a, 4). Only at very high x_{Sr}, the data suggest $x_{Sr}^{lawsonite} > x_{Sr}^{aqueous\ fluid}$ (Fig. 4). Within the precision of our data, fractionation behavior of orthorhombic and monoclinic lawsonite appears to be similar (Fig. 4). The site dependent Ca-Sr fractionation between zoisite and aqueous fluid is very strong (Fig. 3b). While the larger A2 site shows practically no Ca-Sr fractionation with $x_{Sr}^{zoisite\ A2} \sim x_{Sr}^{aqueous\ fluid}$ and $K_{D(Sr-Ca)}^{zoisite\ A2-aqueous\ fluid} \sim$

1, the Ca-Sr fractionation between zoisite A1 and aqueous fluid is much more pronounced with $x_{\mathrm{Sr}}^{\text{zoisite A1}} << x_{\mathrm{Sr}}^{\text{aqueous fluid}}$ and an overall $K_{D(Sr-Ca)}^{zoisite\ A1-aqueous\ fluid} \sim 0.05$.

DISCUSSION

Attainment of equilibrium

To derive Ca-Sr fractionation data it is essential to show that the runs reached near-equilibrium conditions. Unfortunately, in empirical work equilibrium may only be assumed or judged based on the absence of disequilibrium features and is only valid unless proven otherwise. Arguments for equilibrium include: i) within errors the derived data sets for zoisite and lawsonite, respectively, are internally consistent (for disequilibrium experiments one would expect scatters or internal inconsistencies within the different data sets), ii) Rietveld refinements of the XRD data yielded good refinement statistics (for disequilibrium experiments one would expect scattered or zoned Ca-Sr compositions in the minerals, which would result in poorer refinement statistics), iii) microprobe data give no hints to any zonation in individual zoisite or lawsonite grains nor to scattered compositions of zoisite or lawsonite in individual runs (see Dörsam et al. 2007 and Liebscher et al. 2010 for more details), and iv) duplicate runs Au31/Pt4, Au29/Pt3, and Au23/Pt2 for zoisite and Au37/Au86 and Au38/Au87 for lawsonite yielded consistent results at least within the precision of our experiments. However, in some of our experiments additional phases formed, which may put doubts on the assumption of equilibrium. Nevertheless, in none of the runs the number of phases violates the phase rule. In run Au29, which was prepared with $SrSiO_3$ as starting material, we observed a large number of phases while in duplicate run Pt3, which was prepared with Sr-hydroxide instead of $SrSiO_3$ as starting material, only zoisite and quartz formed (Table 1a), indicating metastable phases for Au29. However, additional metastable phases should only influence the modal amounts of product phases by shifting the effective bulk composition; additional phases should not influence the Ca-Sr fractionation as long as these additional

311 phases do not change the physico-chemical properties and speciation in the aqueous fluid.
312 Overall, as we have no hints to disequilibrium (at least within the errors of our data) it is
313 probably reasonable and justified to assume equilibrium conditions at least with respect to the
314 Ca-Sr fractionation. Also, in all our previous studies on solid-aqueous fluid element
315 fractionation determined via the applied synthesis experiments, we did not find any evidence
316 for disequilibrium.
317
318 **Thermodynamic evaluation**
319 At constant temperature and pressure and assuming thermodynamic equilibrium, homovalent
320 one-site exchange reactions as (2a), (2b) and (3) can be described thermodynamically by

321 $$\Delta G = 0 = \Delta\mu^0 + RTln\frac{a_{Ca}^{solid} * a_{Sr}^{aqueous\ fluid}}{a_{Sr}^{solid} * a_{Ca}^{aqueous\ fluid}} \quad (4)$$

322 where a_i is the activity of component *i* in solid solution and aqueous fluid, respectively, and
323 $\Delta\mu^0$ the difference in standard chemical potentials between products and educts of reactions
324 (2a), (2b) and (3), respectively. With the definition of activity $a_i = x_i * \gamma_i$ equation (4)
325 transforms into

326 $$0 = \Delta\mu^0 + RTln\frac{x_{Ca}^{solid} * x_{Sr}^{aqueous\ fluid}}{x_{Sr}^{solid} * x_{Ca}^{aqueous\ fluid}} + RTln\frac{\gamma_{Ca}^{solid} * \gamma_{SSr}^{aqueous\ fluid}}{\gamma_{Sr}^{solid} * \gamma_{Ca}^{aqueous\ fluid}}. \quad (5)$$

327 For the 1 M (Ca,Sr)Cl_2 aqueous solutions used in this study one may reasonably well assume
328 that Henry´s law applies for the fluid and $\gamma_i = k_i$. For simplicity and due to the chemical
329 similarity of both species we assume that Henry´s constants for Sr^{2+} and Ca^{2+} equal each
330 other. Additionally applying the definition for the exchange coefficient

331 $$K_{D(Sr-Ca)}^{solid-aqueous\ fluid} = \frac{x_{Ca}^{solid} * x_{Sr}^{aqueous\ fluid}}{x_{Sr}^{solid} * x_{Ca}^{aqueous\ fluid}} \quad (6)$$

332 equation (5) simplifies to

333 $$0 = \Delta\mu^0 + RTlnK_{D(Sr-Ca)}^{solid-aqueous\ fluid} + RTln\frac{\gamma_{Ca}^{solid}}{\gamma_{Sr}^{solid}}. \quad (7)$$

While the exchange coefficient can be extracted from the experimental data, calculation of the activity coefficient requires an activity model. The simplest activity model for binary homovalent one-site mixing is that of a regular solution for which

$$RTln\gamma_{Ca}^{solid} = {x_{Sr}^{solid}}^2 * W_{Sr-Ca}^{solid} \qquad (8a)$$

and

$$RTln\gamma_{Sr}^{solid} = {x_{Ca}^{solid}}^2 * W_{Sr-Ca}^{solid} . \qquad (8b)$$

Combining and re-arranging equation (7) with equations (8a) and (8b) and formulating explicitly for exchange reactions (2a), (2b) and (3) yield

$$-lnK_{D(Sr-Ca)}^{zoisite\ A1-aqueous\ fluid} = \frac{1}{RT}\Delta\mu^0 + \frac{1}{RT}W_{Sr-Ca}^{zoisite\ A1} * \left(x_{Sr^{A1}-zoisite}^{zoisite} - x_{Ca^{A1}-zoisite}^{zoisite}\right), \qquad (9a)$$

$$-lnK_{D(Sr-Ca)}^{zoisite\ A2-aqueous\ fluid} = \frac{1}{RT}\Delta\mu^0 + \frac{1}{RT}W_{Sr-Ca}^{zoisite\ A2} * \left(x_{Sr^{A2}-zoisite}^{zoisite} - x_{Ca^{A2}-zoisite}^{zoisite}\right) \qquad (9b)$$

and

$$-lnK_{D(Sr-Ca)}^{lawsonite-aqueous\ fluid} = \frac{1}{RT}\Delta\mu^0 + \frac{1}{RT}W_{Sr-Ca}^{lawsonite} * \left(x_{Sr-lawsonite}^{lawsonite} - x_{Ca-lawsonite}^{lawsonite}\right). \qquad (10)$$

Diagrams of $-lnK_{D(Sr-Ca)}^{mineral-aqueous\ fluid}$ versus $\left(x_{Sr-mineral}^{mineral} - x_{Ca-mineral}^{mineral}\right)$ therefore should result in linear relations with an intercept of $\frac{1}{RT}\Delta\mu^0$ and a slope of $\frac{1}{RT}W_{Sr-Ca}^{mineral}$; within the precision of our data, the experimental results fulfill this linear relationship (Fig. 5). To extract $\Delta\mu^0$ and $W_{Sr-Ca}^{mineral}$ at P and T of our experiments from equations (9a), (9b) and (10) we only fitted the data derived at 2 GPa/600 °C for zoisite and 4 GPa/600 °C for lawsonite. However, within experimental and analytical errors the results from the other runs are consistent with the derived linear fits. Evaluation of the data yields $\Delta\mu^0$ = -29 kJ/mol and $W_{Sr-Ca}^{zoisite\ A1}$ = 5.5 kJ/mol for Ca-Sr fractionation between aqueous fluid and zoisite A1 site, $\Delta\mu^0$ = -1.1 kJ/mol and $W_{Sr-Ca}^{zoisite\ A2}$ = 0 kJ/mol for Ca-Sr fractionation between aqueous fluid

and zoisite A2 site, $\Delta\mu^0$ = -10 kJ/mol and $W_{Sr-Ca}^{lawsonite\ P21/m}$ = 11 kJ/mol for Ca-Sr fractionation between aqueous fluid and monoclinic lawsonite, and $\Delta\mu^0$ = -9 kJ/mol and $W_{Sr-Ca}^{lawsonite\ Cmcm}$ = 10 kJ/mol for Ca-Sr fractionation between aqueous fluid and orthorhombic lawsonite. The derived values for zoisite reflect the strong intracrystalline Ca-Sr fractionation between A1 and A2 sites in zoisite. For the A2 site the data indicate ideal behavior of the Ca-Sr solid solution as well as almost identical standard state chemical potentials for the Ca^{A2}- and Sr^{A2}-endmembers. For most natural systems with low x_{Sr}^{bulk}, the Sr concentration in zoisite will be exclusively controlled by Sr incorporation on the A2 site. Consequently, due to the ideal behavior of the A2 site, $x_{Sr}^{zoisite\ A2}$ can reasonably well be taken representative of the coexisting $x_{Sr}^{aqueous\ fluid}$. For orthorhombic and monoclinic lawsonite the data indicate almost identical energetics of the Ca-Sr substitution.

Calculation of Nernst distribution coefficients

To allow comparison of our data with those published by Feineman et al. (2007) and Martin et al. (2011) we use our data to calculate the corresponding Nernst distribution coefficients for the Sr-partitioning between aqueous fluid and zoisite and lawsonite. The Nernst distribution coefficient is typically used to describe the trace element partitioning between coexisting phases α and β based on the concentration c as $D_i^{\alpha\text{-}\beta} = c_i^{\alpha}/c_i^{\beta}$. However, one has to be aware that in a strict sense any D-value is only valid for the P-T-x conditions for which it has been determined. We used the x_{Sr} data derived in this study to calculate the corresponding Sr concentrations in zoisite, lawsonite and aqueous fluid, assuming stoichiometric compositions of (Ca,Sr)-zoisite and (Ca,Sr)-lawsonite and the 1 M $(Ca,Sr)Cl_2$ aqueous solution (Fig. 6). The concentrations $c_{Sr}^{zoisite}$ and $c_{Sr}^{aqueous\ fluid}$ are linearly correlated up to about $c_{Sr}^{zoisite}$ ~ 17 wt% (equivalent to $x_{Sr}^{zoisite}$ ~ 0.5) and $c_{Sr}^{aqueous\ fluid}$ ~ 6.6 wt% (equivalent to $x_{Sr}^{aqueous\ fluid}$ ~ 0.8) (Fig. 6a). For lawsonite, such a linear relation between $c_{Sr}^{lawsonite}$ and $c_{Sr}^{aqueous\ fluid}$ is observed for a much more restricted compositional range of up to about $c_{Sr}^{lawsonite}$ ~ 1.5 wt% (equivalent to

384 $x_{Sr}^{lawsonite} \sim 0.06$) and $c_{Sr}^{aqueous\ luid} \sim 2.0$ wt% (equivalent to $x_{Sr}^{aqueous\ fluid} \sim 0.24$) (Fig. 6b).
385 Fitting those data for a linear relation between $c_{Sr}^{mineral}$ and $c_{Sr}^{aqueous\ fluid}$ forced through the
386 origin yields $D_{Sr}^{zoisite\text{-}aqueous\ fluid} = 2.8 \pm 0.7$ and $D_{Sr}^{lawsonite\text{-}aqueous\ fluid} = 0.6 \pm 0.2$ (Fig. 6c). The
387 derived $D_{Sr}^{zoisite\text{-}aqueous\ fluid}$ value fits perfectly with the results by Martin et al. (2011) who
388 determined $D_{Sr}^{zoisite\text{-}aqueous\ fluid} = 2.2 \pm 0.3$ to 3.6 ± 1.2, while the derived $D_{Sr}^{lawsonite\text{-}aqueous\ fluid}$ is
389 slightly higher than that derived by Martin et al. (2011) with $D_{Sr}^{lawsonite\text{-}aqueous\ fluid} = 0.14 \pm 0.02$
390 to 0.20 ± 0.02. Our data supports the findings by Martin et al. (2011) that Sr is compatible in
391 zoisite and incompatible in lawsonite. The notably higher $D_{Sr}^{zoisite\text{-}aqueous\ fluid}$ values of 42 ± 18
392 to 170 ± 80 determined by Feineman et al. (2007) cannot be explained with the data at hand.
393 Their experiments were performed at slightly higher temperatures of 750 to 900 °C compared
394 to this study. However, these only slightly higher temperatures can reasonably well be
395 excluded as being responsible for the more than 10- to 50-times higher $D_{Sr}^{zoisite\text{-}aqueous\ fluid}$
396 values determined by Feineman at el. (2007). The experiments by Feineman et al. (2007) were
397 performed with Fe-bearing zoisite with ~ 1 wt% Fe_2O_3 compared to the Fe-free system
398 studied here. Incorporation of Fe in the M3 octahedron affects the crystal-structural properties
399 of the A1 and A2 sites (Liebscher et al. 2002) and by this may influence the Ca-Sr
400 fractionation. However, Liebscher et al. (2002) also have shown that the structural changes of
401 A1 and A2 with increasing Fe-content are only minor, at least for low Fe contents. So the
402 effect of Fe on Sr incorporation should also be minor.
403
404 **Application to natural systems**
405 An example of fluid-induced Sr metasomatism was reported by Brastadt (1985) from a
406 retrogressed metaeclogite from Bjørkedalen, Norway. Besides relicts of the eclogitic
407 assemblage, this rock is predominantly composed of hornblende, plagioclase, Fe/Ti oxides
408 and apatite and shows clear evidence of a second alteration stage caused by the infiltration of
409 an external aqueous fluid from the neighboring lithologies. This second alteration stage

essentially resulted in the hydration and breakdown of plagioclase to epidote, thomsonite, and variable amounts of zoisite, clinozoisite, prehnite, sphene, smectite, calcite, paragonite and Sr-feldspar. Whole rock and mineral analyses indicate that the infiltrating aqueous fluid also added Sr to the rock. The different epidote group minerals are characterized by high Sr contents. Maximum Sr contents reported by Brastad (1985) are 8.52 wt% SrO in epidote, 4.73 wt% SrO in clinozoisite and 7.42 wt% SrO in zoisite. Assuming exclusive incorporation of Sr on the respective A2 sites as indicated by our data, these concentrations transfer to $x_{Sr}^{\text{epidote A2}} = 0.402$, $x_{Sr}^{\text{clinozoisite A2}} = 0.217$, and $x_{Sr}^{\text{zoisite A2}} = 0.333$. Applying $K_{D(Sr-Ca)}^{epidote\ mineral\ A2-aqueous\ fluid} = 1$ as determined here for zoisite yields minimum molar Ca/Sr ratios in the aqueous fluid of 1.5 based on epidote, 3.6 based on clinozoisite and 2.0 based on zoisite. These values agree well with those determined by Najorka et al. (1999) for the Ca/Sr ratio in the Bjørkedalen fluid of 1.8 and 1.7 based on the Sr-contents in plagioclase as given by Brastad (1985) and the plagioclase-fluid distribution data by Lagache & Dujon (1987) and Kotelnikov et al. (1989), respectively. Using the Nernst distribution coefficient for zoisite-aqueous fluid derived in this study the calculated Sr concentration in the Bjørkedalen fluid is 2.2 (1.8 to 3.0) wt%.

A detailed mass-balancing of the Sr-cycle in subduction zones is beyond the scope of this paper. However, some general conclusions and speculations can be drawn from the Ca-Sr fractionation behavior determined here. Our data show that Sr is incompatible in lawsonite but compatible in zoisite, consistent with previously published data. In cold, lawsonite-bearing subduction zone settings any upward migrating aqueous fluid will therefore strip-off Sr out of the lawsonite-bearing rock resulting in a progressively Sr-depleted residue. Due to this progressive Sr-depletion, fluids formed at greater depths in such cold, lawsonite-bearing subduction zone settings will exhibit continuously decreasing Sr concentrations. Contrary, in warm, zoisite-bearing subduction zone settings the rocks will act as a sink for Sr and strip-off Sr out of the upward migrating fluid resulting in a progressively Sr-enriched residue. Due to

436 this progressive Sr-enrichment, fluids formed at greater depths in such warm, zoisite-bearing
437 subduction zone settings will exhibit continuously increasing Sr concentrations.
438

439 **Acknowledgements**

440 This paper greatly benefitted from careful and critical reviews by M. Feineman and an
441 anonymous reviewer. Critical and constructive editorial handling by E. Ghent is gratefully
442 acknowledged.
443

References

Brastad, K. (1985) Sr metasomatism, and partition of Sr between the mineral phases of a meta-eclogite from Bjorkedalen, West Norway. Tschermaks Mineralogische und Petrographische Mitteilungen, 34, 87–103.

Caglioti, G., Paoletti, A., and Ricci, F.P. (1958) Choice of collimators for crystal spectrometer for neutron diffraction. Nuclear Instruments, 3, 223-228.

Dörsam, G., Liebscher, A., Wunder, B., Franz, G.,and Gottschalk, M. (2007) Crystal chemistry of synthetic $Ca_2Al_3Si_3O_{12}OH$ - $Sr_2Al_3Si_3O_{12}OH$ solid-solution series of zoisite and clinozoisite. American Mineralogist, 92, 1133-1147.

Feineman, M.D., Ryerson, F.J., DePaolo, D.J., and Plank, T. (2007) Zoisite-aqueous fluid trace element partitioning with implications for subduction zone fluid composition. Chemical Geology, 239, 250-265.

Grapes, R. and Watanabe, T. (1984) Al-Fe^{3+} and Ca-Sr^{2+} epidotes in metagreywacke-quartzofeldspathic schist, Southern Alps, New Zealand. American Mineralogist, 69, 490-498.

Kotelnikov, A.R., Chernysheva, I.V., Romanenko, I.M., and Tikhomirova, E.I. (1989) Experimental determination of energy of mixing of Ca-Sr-anorthites from data on cation-exchange equilibria. Geochimia, 11, 1575-1586.

Lagache, M. and Dujon, S.C. (1987) Distribution of strontium between plagioclases and 1 molar aqueous chloride solutions at 600 °C, 1.5 kbar and 750 °C, 2 kbar. Bulletin Mineralogie, 110, 551-561.

Larson, A.C. and Von Dreele, R.B. (2000) General structure analysis system (GSAS). Los Alamos National Laboratory Report LAUR, 86-748.

Libowitzky, E. and Armbruster, Th. (1995) Low-temperature phase transitions and the role of hydrogen bonds in lawsonite. American Mineralogist, 80, 1277-1285.

Liebscher, A., Gottschalk, M., and Franz, G. (2002) The substitution Fe3+-Al and the isosymmetric displacive phase transition in synthetic zoisite: A powder X-ray and infrared spectroscopy study. American Mineralogist, 87, 909-921.

Liebscher, A., Thiele, M., Franz, G., Dörsam, G., and Gottschalk, M. (2009) Synthetic Sr-Ca margarite, anorthite and slawsonite solid solutions and solid-fluid Sr-Ca fractionation. European Journal of Mineralogy, 21, 275-292.

Liebscher, A., Dörsam, G., Franz, G., Wunder, B., and Gottschalk, M. (2010) Crystal chemistry of synthetic lawsonite solid-solution series $CaAl_2[(OH)_2/Si_2O_7] \bullet H_2O$ - $CaAl_2[(OH)_2/Si_2O_7] \bullet H_2O$ and the *Cmcm-P*2_1*/m* phase transition. American Mineralogist, 95, 724-735.

Martin, L.A.J., Wood, B., Turner, S., and Rushmer, T. (2011) Experimental measurements of trace element partitioning between lawsonite, zoisite and fluid and their implication for the composition of arc magmas. Journal of Petrology, 52, 1049-1075.

Massonne, H.-J. and Schreyer, W. (1986) High-pressure syntheses and X-ray properties of white micas in the system K_2O-MgO-Al_2O_3-SiO_2-H_2O. Neues Jahrbuch für Mineralogie, Abhandlungen, 153, 177-215.

Miyajima, H., Matsubara, S., Miyawaki, R., and Ito, K. (1999) Itoigawaite, a new mineral, the Sr analogue of lawsonite, in jadeitite from the Itoigawa-Ohmi district, central Japan. Mineralogical Magazine, 63, 909-916.

Miyajima, H., Matsubara, S., Miyawaki, R., and Horikawa, K. (2002) Niigataite, $CaSrAl_3(Si_2O_7)(SiO_4)O(OH)$: Sr-analogue of clinozoisite, a new member of the epidote group from the Itoigawa-Ohmi district, Niigata Prefecture,central Japan. Journal of Mineralogical and Petrological Science, 98, 118-129.

Nagasaki, A. and Enami, M. (1998) Sr-bearing zoisite and epidote in ultra-high pressure (UHP) metamorphic rocks from the Su-Lu province, eastern China: an important Sr reservoir under UHP conditions. American Mineralogist, 83, 240-247.

Najorka, J., Gottschalk, M., Franz, G., and Heinrich, W. (1999) Ca-Sr distribution among amphibole, clinopyroxene, and chloride-bearing solutions. American Mineralogist, 84, 596-606.

Pawley, A.R. and Allan, D.R. (2001) A high-pressure study of lawsonite using angle-dispersive powder-diffraction methods with synchrotron radiation. Mineralogical Magazine, 65, 41-58.

Pouchou, J.L. and Pichoir, F. (1984) Un nouveau modèle de calcul pour la microanalyse quantitative par spectrométrie de rayons X. La Recherche Aérospatiale, 3, 167-192.

Shannon, R.D. (1976) Revised ionic radii and systematic studies of interatomic distances in halides and chalcogenides. Acta Crystallographica, A32, 751–767.

Spandler, C., Hermann, J., and Arculus, R. (2003) Redistribution of trace elements during prograde metamorphism from lawsonite blueschist to eclogite facies; implications for deep subduction-zone processes. Contribution to Mineralogy and Petrology, 146, 205-222.

Tribuzio, R., Messiga, B., Vannucci, R., and Bottazzi, P. (1996) Rare earth element redistribution during high-pressure-low-temperature metamorphism in ophiolitic Fe-gabbros (Liguria, northwestern Italy); implications for light REE mobility in subduction zones. Geology, 24, 711-714.

Zack, T., Foley, S.F., and Rivers, T. (2002) Equilibrium and Disequilibrium Trace Element Partitioning in Hydrous Eclogites (Trescolmen, Central Alps). Journal of Petrology, 43, 1947-1974.

Zimmermann, R., Heinrich, W., and Franz, G. (1996) Tremolite synthesis from $CaCl_2$-bearing aqueous solutions. European Journal of Mineralogy, 8, 767-776.

519 **Figure captions**

520

521 **Figure 1**: Ca-Sr composition of run products expressed as $x_{Sr} = n_{Sr}/(n_{Sr} + n_{Ca})$ versus x_{Sr}^{bulk} for
522 zoisite (A) and coexisting aqueous fluid (B) and lawsonite (C) and coexisting aqueous fluid
523 (D). Overall the data indicate $x_{Sr}^{solid} \leq x_{Sr}^{bulk}$ and $x_{Sr}^{aqueous\ fluid} > x_{Sr}^{bulk}$ and suggest preferred
524 fractionation of Sr over Ca into the aqueous fluid.

525

526 **Figure 2**: Intracrystalline Ca-Sr fractionation between zoisite A1 and A2 sites. The data
527 indicate notable intracrystalline fractionation with a clear preference of Sr for the larger A2
528 site. Up to $x_{Sr}^{zoisite} \sim 0.4$ Sr is almost exclusively incorporated in the A2 site, only for higher Sr
529 concentrations notable amounts of Sr can be found on the A1 site (A). Most data are
530 consistent with an intracrystalline exchange coefficient $K_{D(Sr-Ca)}^{A1-A2}$ = 10 to 20 (B).

531

532 **Figure 3**: Ca-Sr fractionation between zoisite and aqueous fluid (A) as well as the site
533 dependent Ca-Sr fractionation between zoisite A1 and A2 sites and aqueous fluid (B). The site
534 dependent Ca-Sr fractionation shows $K_{D(Sr-Ca)}^{zoisite\ A1-aqueous\ fluid} \sim 0.05$ and
535 $K_{D(Sr-Ca)}^{zoisite\ A2-aqueous\ fluid} \sim 1$ reflecting the notable intracrystalline fractionation. Due to the
536 preferred substitution of Sr on the A2 site, the data suggest that for low x_{Sr}^{bulk}, as may be
537 assumed for most natural systems, $x_{Sr}^{aqueous\ fluid} = x_{Sr}^{zoisite\ A2}$.

538

539 **Figure 4**: Ca-Sr fractionation between monoclinic (A) and orthorhombic (B) lawsonite and
540 aqueous fluid. Except for high x_{Sr} the data indicate preference of Sr over Ca for the aqueous
541 fluid.

542

543 **Figure 5**: Thermodynamic evaluation of the Ca-Sr solid-fluid fractionation for zoisite-A1 site
544 (A), zoisite-A2 site (B), monoclinic (C) and orthorhombic (D) lawsonite expressed as
545 $-lnK_{D(Sr-Ca)}^{mineral-aqueous\ fluid}$ versus $\left(x_{Sr-mineral}^{mineral} - x_{Ca-mineral}^{mineral}\right)$ diagrams. Linear fits in (A)
546 and (B) based on data at 2 GPa/600 °C, those in (C) and (D) based on data at 4 GPa/600 °C.
547 Data indicate ideal behavior of the Ca-Sr substitution on zoisite A2 site. Monoclinic and
548 orthorhombic lawsonite exhibit comparable Ca-Sr substitution behavior.
549
550 **Figure 6**: Calculated Sr-concentrations in coexisting zoisite and aqueous fluid (a) and
551 lawsonite and aqueous fluid (b). Concentrations are calculated based on the x_{Sr} values
552 determined in this study and assuming stoichiometric composition in zoisite and lawsonite
553 and a 1 M $(Ca,Sr)Cl_2$ aqueous fluid. The grey shaded area for low Sr-concentrations is
554 enlarged in (c) showing only data for zoisite at 2 GPa/600 °C and for orthorhombic lawsonite
555 at 4 GPa/600 °C. Stippled lines in (a) and (b) are drawn by eye while stippled lines in (c) are
556 linear fits to the data forced through the origin. The slope of these fits yields the Nernst
557 distribution coefficients $D_{Sr}^{\text{mineral-aqueous fluid}}$ with $D_{Sr}^{\text{zoisite-aqueous fluid}} = 2.8 \pm 0.7$ and $D_{Sr}^{\text{lawsonite-}}$
558 $^{\text{aqueous fluid}} = 0.6 \pm 0.2$.
559

Table 1a. Experimental conditions, run products, Ca-Sr composition of zoisite and aqueous fluid, and calculated exchange coefficients K_D for A-site specific Ca-Sr exchange between zoisite and aqueous fluid.

Run	**Pt84**	**Pt85**	**Au32** [1)]	**Pt9**	**Au45** [1)]	**Au31** [1)]	**Pt4** [1)]
P [GPa]	2	2	2	2	2	2	2
T [°C]	550	550	600	600	600	600	600
Phase	zo+qtz	zo+qtz	zo+qtz	zo+qtz	zo+qtz	zo+qtz	zo+qtz
x_{Sr}^{bulk}	0.10	0.14	0.0625	0.125	0.18	0.25	0.25
Starting material							
SiO_2 [mg]	6.64	6.66	6.43	4.97	5.63	5.61	5.23
Al_2O_3 [mg]	5.36	5.38	5.16	3.84	4.87	5.10	4.04
$Ca(OH)_2$ [mg]	4.68	4.48	4.69	3.79	3.87	3.71	2.93
$SrSiO_3$ [mg]	/	/	0.69	1.94	1.88	2.73	/
$Sr(OH)_2$-8 H_2O	1.86	2.62	/	/	/	/	3.51
Fluid [mg] [2)]	2.05	2.49	5.85	5.17	6.29	5.78	5.27
Solid run products							
quartz/coesite [3)]	1.6	0.7	5	6.4	/	5	/
zoisite	30	17	45	48	53	48	100
clinozoisite	49	74	50	45	47	47	/
lawsonite $P2_1/m$	/	/	/	/	/	/	/
lawsonite $Cmcm$	/	/	/	/	/	/	/
strontianite	/	0.2	/	/	/	/	/
kyanite	/	/	/	0.3	/	/	/
Total [4)]	99.6	98.9	100	99.7	100	100	100
Composition [5)]							
$x_{Sr}^{zoisite}$	0.05 (3)	0.19 (9)	0.06 (2)	0.16 (5)	0.16 (3)	0.25 (3)	0.22 (1)
$x_{Sr}^{zoisite\ A1}$	0.03 (3)	0.10 (9)	0.02 (2)	0.07 (5)	0.03 (2)	0.06 (2)	0.03 (1)
$x_{Sr}^{zoisite\ A2}$	0.06 (3)	0.27 (8)	0.09 (3)	0.24 (5)	0.29 (3)	0.44 (3)	0.40 (1)
Ca^{2+} [mmol]	0.0017	0.0016	0.006	0.0037	0.0045	0.0012	0.0044
Sr^{2+} [mmol]	0.0005	0.0006	0.0009	0.0013	0.0025	0.0007	0.0014
$x_{Sr}^{aqueous\ fluid}$	0.23 (1)	0.27 (1)	0.13 (1)	0.26 (1)	0.36 (2)	0.37 (2)	0.24 (1)
$K_{D(Sr-Ca)}^{zoisite\ A1-aqueous\ fluid}$ [6)]	9.51	3.38	7.35	4.67	17.96	9.14	10.29
$K_{D(Sr-Ca)}^{zoisite\ A2-aqueous\ fluid}$ [7)]	4.61	1.01	1.52	1.11	1.36	0.74	0.48

(continued)

Table 1a (cont.)

Run	**Au42** [1)]	**Au29**	**Pt3** [1)]	**Au43** [1)]	**Au23** [1)]	**Pt2** [1)]	**Au22** [1)]
P [GPa]	2	2	2	2	2	2	2
T [°C]	600	600	600	600	600	600	600
Phase	zo+qtz	zo+qtz	zo+qtz	zo+qtz	zo+qtz	zo+qtz	zo+qtz
x_{Sr}^{bulk}	0.4	0.5	0.5	0.65	0.75	0.75	0.875
Starting material							
SiO_2 [mg]	5.01	4.59	5.05	4.02	3.52	4.66	2.16
Al_2O_3 [mg]	5.10	5.08	3.90	5.11	4.98	3.59	3.54
$Ca(OH)_2$ [mg]	2.96	2.46	1.89	1.73	0.91	0.87	0.33
$SrSiO_3$ [mg]	4.37	5.44	/	7.11	8.00	/	6.64
$Sr(OH)_2$-8 H_2O	/	/	6.77	/	/	9.36	/
Fluid [mg] [2)]	5.77	5.73	5.33	6.05	5.73	5.41	1.27
Solid run products							
quartz/coesite [3)]	1	1.6	2	6	4	1	31
zoisite	41	12	98	33	69	92	59
clinozoisite	58	53	/	40	/	/	/
lawsonite $P2_1/m$	/	26	/	18	23	/	4
lawsonite *Cmcm*	/	1.5	/	/	/	/	/
strontianite	/	1.2	/	3	2	7	6
kyanite	/	4.3	/	/	/	/	/
Total [4)]	100	99.6	100	100	98	100	100
Composition [5)]							
$x_{Sr}^{zoisite}$	0.37 (3)	0.37 (10)	0.42 (1)	0.55 (3)	0.66 (4)	0.63 (2)	0.77 (2)
$x_{Sr}^{zoisite\ A1}$	0.09 (3)	0.08 (8)	0.13 (1)	0.19 (3)	0.41 (3)	0.38 (1)	0.61 (2)
$x_{Sr}^{zoisite\ A2}$	0.67 (3)	0.66 (10)	0.72 (1)	0.82 (4)	0.92 (4)	0.89 (2)	0.93 (3)
Ca^{2+} [mmol]	0.0019	0.0007	0.0005	0.0014	0.0003	0.0003	0.0001
Sr^{2+} [mmol]	0.004	0.0014	0.0023	0.0063	0.0033	0.0024	0.0006
$x_{Sr}^{aqueous\ fluid}$	0.68 (3)	0.67 (3)	0.82 (4)	0.82 (4)	0.92 (5)	0.89 (4)	0.86 (4)
$K_{D(Sr-Ca)}^{zoisite\ A1-aqueous\ fluid}$ [6)]	21.29	23.0	30.78	19.18	15.83	13.05	3.84
$K_{D(Sr-Ca)}^{zoisite\ A2-aqueous\ fluid}$ [7)]	1.04	1.03	1.79	0.99	0.96	0.99	0.45

(continued)

Table 1a (cont.)

Run	Au33 [1)]	Au44 [1)]	Au84	Pt103	Pt106
P [GPa]	2	2	2	4	4
T [°C]	600	600	700	800	800
Phase	zo+qtz	zo+qtz	fsp+qtz	law+coe	law+coe
x_{Sr}^{bulk}	0.95	0.95	0.875	0.051	0.14
Starting material					
SiO_2 [mg]	2.69	2.63	5.82	5.84	6.43
Al_2O_3 [mg]	4.88	4.78	7.75	4.72	5.20
$Ca(OH)_2$ [mg]	0.24	0.23	0.70	3.25	3.25
$SrSiO_3$ [mg]	9.93	9.71	10.88	/	/
$Sr(OH)_2$-8 H_2O	/	/	/	0.63	1.90
Fluid [mg] [2)]	11.29	6.60	6.56	5.61	5.70
Solid run products					
quartz/coesite [3)]	2	2	6.2	20	15
zoisite	56	76	31	58	60
clinozoisite	/	/	8	4.8	0.9
lawsonite $P2_1/m$	39	21	/	/	/
lawsonite $Cmcm$	/	/	/	1.9	11.2
strontianite	3	1	2.3	/	/
kyanite	/	/	5.4	14	10
Total [4)]	100	100	99.9	98.7	99.2
Composition [5)]					
$x_{Sr}^{zoisite}$	0.86 (2)	0.87 (2)	0.58 (3)	0.08 (3)	0.14 (3)
$x_{Sr}^{zoisite\ A1}$	0.76 (2)	0.82 (2)	0.32 (4)	0.01 (1)	0.02 (2)
$x_{Sr}^{zoisite\ A2}$	0.96 (2)	0.92 (2)	0.84 (3)	0.15 (3)	0.27 (3)
Ca^{2+} [mmol]	0	0.0001	0.0003	0.0056	0.0046
Sr^{2+} [mmol]	0.0112	0.0062	0.0058	0.0007	0.0026
$x_{Sr}^{aqueous\ fluid}$	1.00 (5)	0.98 (5)	0.95 (5)	0.11 (1)	0.36 (2)
$K_{D(Sr-Ca)}^{zoisite\ A1-aqueous\ fluid}$ [6)]		13.61	41.08	12.375	27.70
$K_{D(Sr-Ca)}^{zoisite\ A2-aqueous\ fluid}$ [7)]		5.39	3.68	0.71	1.53

Note: errors in parentheses refer to 1σ standard deviation

[1)] runs discussed in Doersam et al. (2007) with respect to the orthorhombic and monoclinic $Ca_2Al_3[(O/OH)/SiO_4Si_2O_7] – Sr_2Al_3[(O/OH)/SiO_4Si_2O_7]$ solid solution series

[2)] fluid was an aqueous 1 M $(Ca,Sr)Cl_2$ solution with $x_{Sr}^{fluid} = x_{Sr}^{bulk}$

[3)] coesite in 4 GPa runs

[4)] additional phases are pyrophyllite in Pt84 and Pt85, slawsonite in Au84, and walstromite in Pt106

[5)] Ca-Sr composition of zoisite determined by XRD with Rietveld refinement, mass [mmol] of Ca and Sr in product fluid determined by ICO-OES ; $x_{Sr} = n_{Sr}/(n_{Sr} + n_{Ca})$

[6)] $K_{D(Sr-Ca)}^{zoisite\ A1-aqueous\ fluid} = \frac{x_{Ca^{A1}-zoisite}^{zoisite} * x_{Sr}^{aqueous\ fluid}}{x_{Sr^{A1}-zoisite}^{zoisite} * x_{Ca}^{aqueous\ fluid}}$ according to exchange reaction $Ca^{2+\ (aqueous\ fluid)} + Sr^{(A1)}M^{2+(A2)}Al_3[Si_3O_{11}(O/OH)] = Sr^{2+\ (aqueous\ fluid)} + Ca^{(A1)}M^{2+(A2)}Al_3[Si_3O_{11}(O/OH)]$

[7)] $K_{D(Sr-Ca)}^{zoisite\ A2-aqueous\ fluid} = \frac{x_{Ca^{A2}-zoisite}^{zoisite} * x_{Sr}^{aqueous\ fluid}}{x_{Sr^{A2}-zoisite}^{zoisite} * x_{Ca}^{aqueous\ fluid}}$ according to exchange reaction $Ca^{2+\ (aqueous\ fluid)} + M^{2+(A1)}Sr^{(A2)}Al_3[Si_3O_{11}(O/OH)] = Sr^{2+\ (aqueous\ fluid)} + M^{2+(A1)}Ca^{(A2)}Al_3[Si_3O_{11}(O/OH)]$

Table 1b. Experimental conditions, run products, Ca-Sr composition of orthorhombic and monoclinic lawsonite and aqueous fluid, and calculated exchange coefficients K_D for Ca-Sr exchange between lawsonite and aqueous fluid.

Run	**Pt92**	**Pt93**	**Pt94**	**Au76** [1)]	**Au77** [1)]	**Au78** [1)]	**Au79** [1)]
P [GPa]	2	2	2	4	4	4	4
T [°C]	400	400	400	600	600	600	600
Phase	law+qtz	law+qtz	law+qtz	law+coe	law+coe	law+coe	law+coe
x_{Sr}^{bulk}	0.4	0.6	0.8	0.02	0.03	0.04	0.05
Starting material							
SiO_2 [mg]	6.04	5.09	4.86	12.23	12.11	12.36	12.26
Al_2O_3 [mg]	4.88	4.12	3.92	9.74	9.7	9.94	9.91
$Ca(OH)_2$ [mg]	2.12	1.19	0.57	6.94	6.83	6.93	6.84
$SrSiO_3$ [mg]	5.08	6.43	8.19	0.31	0.47	0.64	0.79
Fluid [mg] [2)]	2.72	2.98	2.5	11.01	11.17	9.33	10.96
Solid run products							
coesite/quartz [3)]	18	19	18	5	7	5	4
lawsonite *P2₁/m*	29	38	43	/	/	/	/
lawsonite *Cmcm*	13.6	11.3	7.9	95	93	95	96
Total [4)]	60.6	68.3	68.9	100	100	100	100
Composition [5)]							
$x_{Sr}^{\text{lawsonite } P21/m}$		0.50 (2)	0.71 (2)				
$x_{Sr}^{\text{lawsonite } Cmcm}$	0.18 (1)	0.62 (5)		0.02 (1)	0.03 (1)	0.04 (2)	0.02 (1)
Ca^{2+} [mmol]	0.002	0.0011	0.0007	0.0086	0.0077	0.0068	0.007
Sr^{2+} [mmol]	0.0019	0.0024	0.0028	0.0008	0.0012	0.0013	0.0017
$x_{Sr}^{\text{aqueous fluid}}$	0.49 (2)	0.69 (3)	0.80 (4)	0.085 (4)	0.135 (7)	0.160 (8)	0.20 (1)
$K_{D(Sr-Ca)}^{lawsonite P2_1/m-aqueous fluid}$ [6)]		2.23	1.67				
$K_{D(Sr-Ca)}^{lawsonite\ Cmcm-aqueous\ fluid}$ [6)]	4.36	1.34		5.07	5.22	5.27	11.32

(continued)

Table 1b. (cont.)

Run	**Au63** [1]	**Au62** [1]	**Au37**	**Au86** [1]	**Au38**	**Au87** [1]	**Au82** [1]
P [GPa]	4	4	4	4	4	4	4
T [°C]	600	600	600	600	600	600	600
Phase	law+coe	law+coe	law+coe	law+coe	law+coe	law+coe	law+coe
x_{Sr}^{bulk}	0.18	0.249	0.4	0.4	0.45	0.45	0.5
Starting material							
SiO_2 [mg]	9.57	9.24	5.96	8.47	5.93	8.54	9.51
Al_2O_3 [mg]	8.69	8.71	5.78	8.21	5.92	8.53	9.78
$Ca(OH)_2$ [mg]	5.18	4.75	2.52	3.58	2.37	3.41	3.55
$SrSiO_3$ [mg]	2.51	3.47	3.71	5.27	4.28	6.16	7.85
Fluid [mg] [2]	5.11	4.37	5.35	10.77	5.02	10.87	10.77
Solid run products							
coesite/quartz [3]	/	1	4.4	7	5.1	5	4
lawsonite *P2₁/m*	57	69	87	87	87	95	96
lawsonite *Cmcm*	42	28	8.8	6	7.5	/	/
Total [4]	99	98	100.2	100	99.6	100	100
Composition [5]							
$x_{Sr}^{lawsonite\ P21/m}$	0.21 (4)	0.32 (2)	0.37 (1)	0.36 (2)	0.41 (1)	0.41 (2)	0.49 (1)
$x_{Sr}^{lawsonite\ Cmcm}$	0.11 (4)	0.19 (0)	0.61 (13)		0.40 (8)		
Ca^{2+} [mmol]	0.0026	0.0019	0.0007	0.0034	0.0017	0.0038	0.0024
Sr^{2+} [mmol	0.003	0.0023	0.0012	0.0057	0.0035	0.0076	0.0053
$x_{Sr}^{faqueous\ fluid}$	0.54 (3)	0.55 (3)	0.63 (3)	0.63 (3)	0.67 (3)	0.67 (3)	0.69 (3)
$K_{D(Sr-Ca)}^{lawsonite P2_1/m-aqueous fluid}$ [6]	4.34	2.57	2.88	2.98	2.97	2.89	2.27
$K_{D(Sr-Ca)}^{lawsonite\ Cmcm-aqueous\ fluid}$ [6]	9.24	5.06	1.12		3.09		

(continued)

Table 1b. (cont.)

Run	Au47 [1)]	Au92 [1)]
P [GPa]	4	4
T [°C]	600	600
Phase	law+coe	law+coe
x_{Sr}^{bulk}	0.65	0.75
Starting material		
SiO_2 [mg]	5.17	5.99
Al_2O_3 [mg]	5.85	7.82
$Ca(OH)_2$ [mg]	1.49	1.42
$SrSiO_3$ [mg]	6.11	9.42
Fluid [mg] [2)]	5.54	4.41
Solid run products		
coesite/quartz [3)]	7	/
lawsonite $P2_1/m$	93	82
lawsonite $Cmcm$	/	/
Total [4)]	100	82
Composition [5)]		
$x_{Sr}^{lawsonite\ P21/m}$	0.63 (1)	0.97 (2)
$x_{Sr}^{lawsonite\ Cmcm}$		
Ca^{2+} [mmol]	0.0008	0.0001
Sr^{2+} [mmol]	0.0025	0.001
$x_{Sr}^{aqueous\ fluid}$	0.77 (4)	0.91 (5)
$K_{D(Sr-Ca)}^{lawsonite P2_1/m-aqueous fluid}$ [6)]	1.86	0.35
$K_{D(Sr-Ca)}^{lawsonite\ Cmcm-aqueous\ fluid}$ [6)]		

Note: errors in parentheses refer to 1σ standard deviation

[1)] runs discussed in Liebscher et al. (2010) with respect to the orthorhombic and monoclinic $CaAl_2[(OH)_2/Si_2O_7]$-H_2O – $SrAl_2[(OH)_2/Si_2O_7]$-H_2O solid solution series

[2)] fluid was an aqueous 1 M $(Ca,Sr)Cl_2$ solution with $x_{Sr}^{fluid} = x_{Sr}^{bulk}$

[3)] quartz in 2 GPa runs

[4)] additional phases are kyanite in Au62, wollastonite in Au62, grossular in Au63 and Au92, clinozoisite in Pt92, and zoisite in Au92; at 2 GPa about 15 wt% strontianite and diaspore each formed in runs Pt92, Pt93 and Pt94

[5)] Ca-Sr composition of lawsonite determined by XRD with Rietveld refinement, mass [mmol] of Ca and Sr in product fluid determined by ICO-OES; $x_{Sr} = n_{Sr}/(n_{Sr} + n_{Ca})$

[6)] $K_{D(Sr-Ca)}^{lawsonite-aqueous\ fluid} = \frac{x_{Ca-lawsonite}^{lawsonite} * x_{Sr}^{aqueous\ fluid}}{x_{Sr-lawsonite}^{lawsonite} * x_{Ca}^{aqueous\ fluid}}$ according to exchange reaction $Ca^{2+\ (aqueous\ fluid)} + SrAl_2[Si_2O_7(OH)_2]\bullet H_2O = Sr^{2+\ (aqueous\ fluid)} + CaAl_2[Si_2O_7(OH)_2]\bullet H_2O$

Liebscher et al., Ca-Sr fractionation
Figure 1

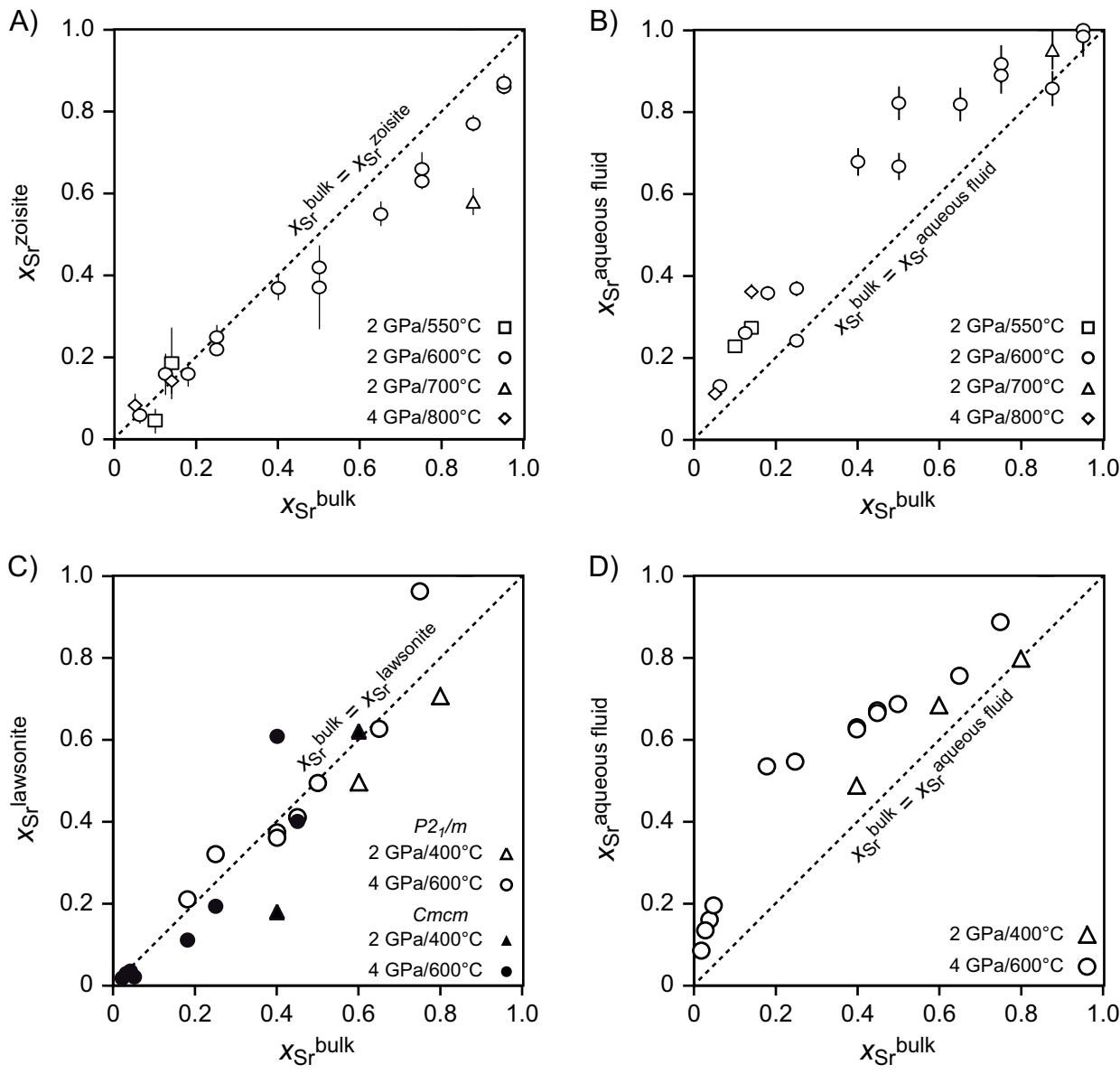

Liebscher et al., Ca-Sr fractionation
Figure 2

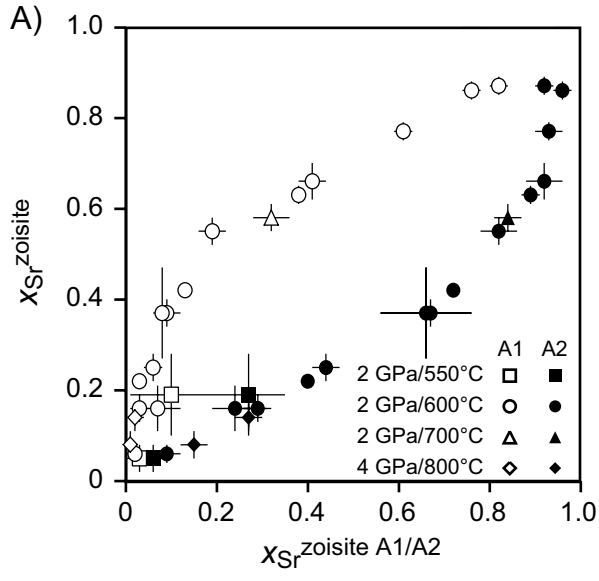

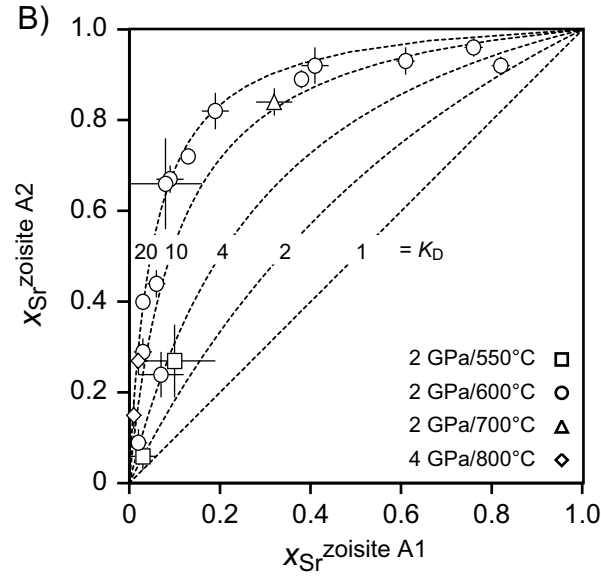

Liebscher et al., Ca-Sr fractionation
Figure 3

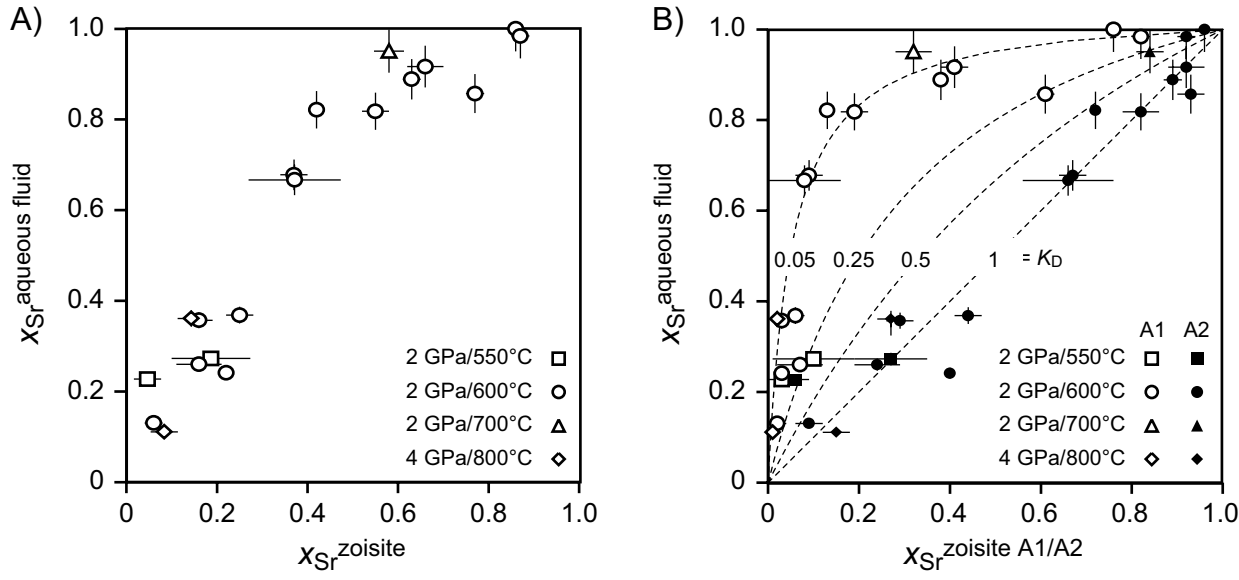

Liebscher et al., Ca-Sr fractionation
Figure 4

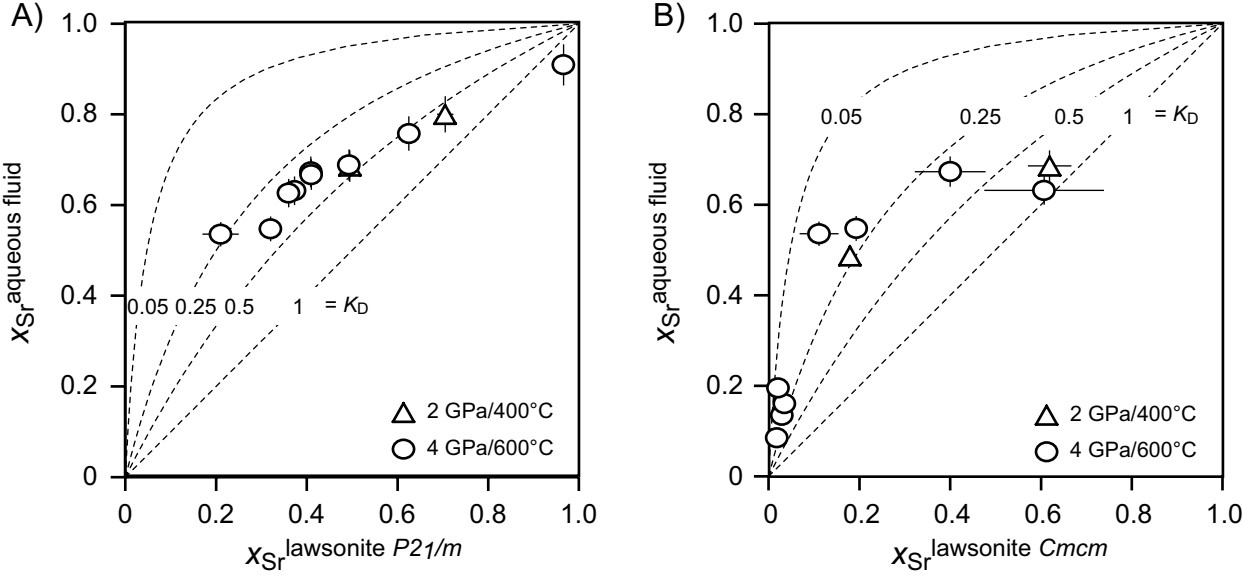

Liebscher et al., Ca-Sr fractionation
Figure 5

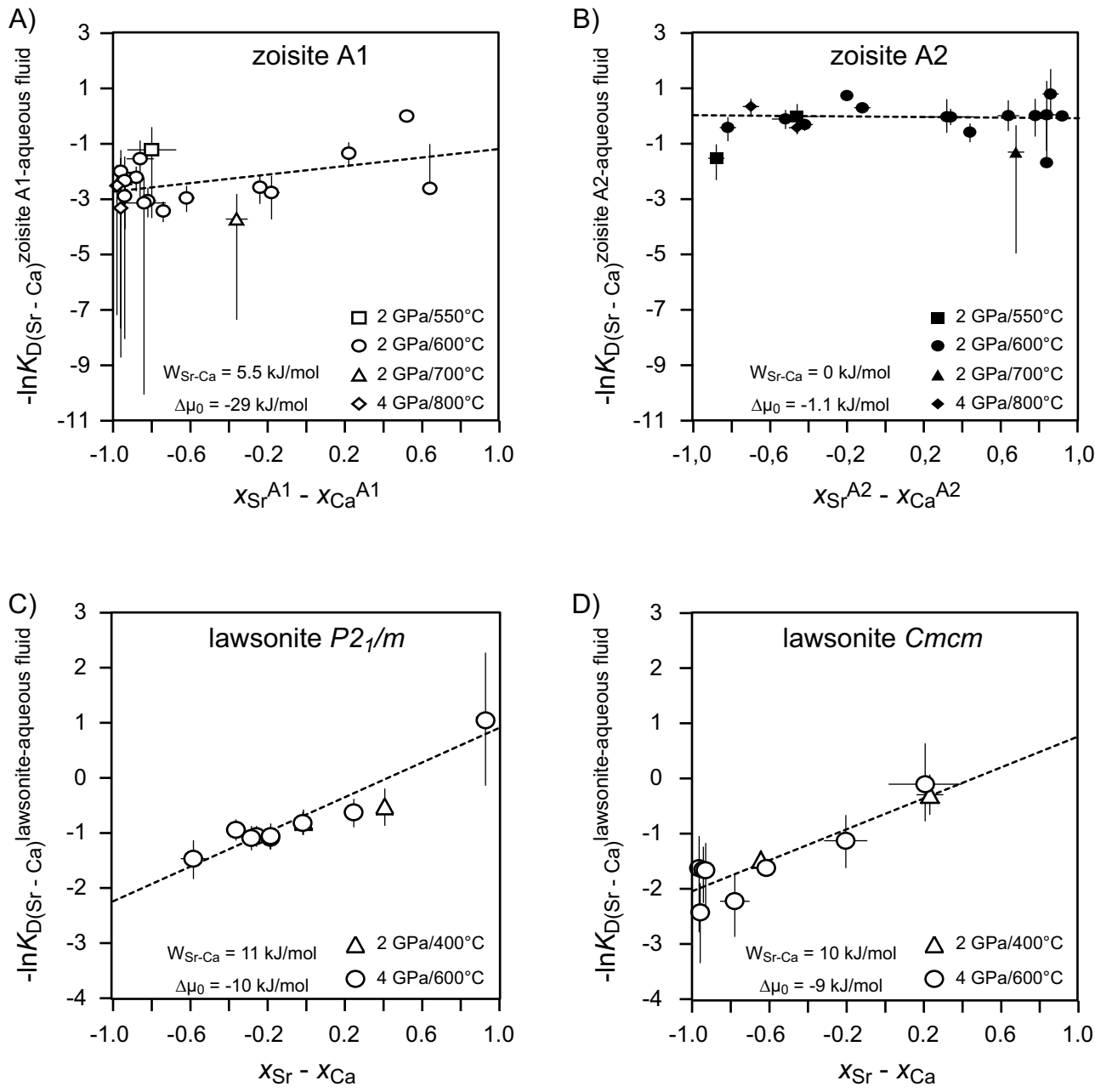

Liebscher et al., Ca-Sr fractionation
Figure 6